Research Article | Vol. 27, No. 5 | 4 Mar 2019 | OPTICS EXPRESS 6471
Optics EXPRESS

Identification of tunneling and multiphoton ionization in intermediate Keldysh parameter regime

RUN WANG,[1] QINGBIN ZHANG,[1,*] DAN LI,[1] SHENGLIANG XU,[1] PENGKUN CAO,[1] YUEMING ZHOU,[1] WEI CAO,[1,3] AND PEIXIANG LU[1,2]

[1] *Wuhan National Laboratory for Optoelectronics and School of Physics, Huazhong University of Science and Technology, Wuhan 430074, China*
[2] *Hubei Key Laboratory of Optical Information and Pattern Recognition, Wuhan Institute of Technology, Wuhan 430205, China*
[3] *weicao@hust.edu.cn*
[*] *zhangqingbin@hust.edu.cn*

Abstract: Quantitative identification of tunneling ionization (TI) and multiphoton ionization (MPI) with Keldysh parameter γ in intermediate regime is of great importance to better understand various ionization-triggered strong-field phenomena. We theoretically demonstrate that the numerical observable ionization delay time is a more reliable indicator for characterizing the transition from TI to MPI under different laser parameters. Using non-linear iterative curve fitting algorithm (NICFA), the detected time-dependent probability current of ionized electrons can be decoupled into weighted TI and MPI portions. This enables us to confirm that the observed plateau-like structure in ionization delay time picture at the intermediate γ originates from the competition between TI and MPI processes. A hybrid quantum and classical approach (HQCA) is developed to evaluate the weights of TI and MPI electrons in good agreement with NICFA result. Moreover, the well separated TI and MPI electrons using HQCA are further propagated classically for mapping their final momentum, which well reproduces the experimental or ab-initio numerical calculated signatures of ionized electron momentum distribution in a rather broad γ regime.

1. Introduction

Ionization is the most fundamental process in strong laser physics, which triggers the successive phenomena, including high order harmonic generation [1–3], above threshold ionization [4–7], as well as ultrafast electron dynamics in semiconductors and dielectrics [8–13]. Since the seminal paper was published in 1964 [14], considerable research efforts have been devoted to this topic, and it is gradually accepted in strong field community that the ionization processes are determined by the Keldysh parameter $\gamma = \omega(2I_p)^{1/2}/E_0$, with the frequency ω, the ionization potential I_p, and the maximum electric field of the laser E_0. With the development of ultrafast laser technology, it is now available for the femtosecond laser's central wavelengths from violet, to near-infrared, even to mid-infrared [15–17], and a large range of intensities from one to eight units of 10^{14} W/cm^2. Therefore, the spanning of γ from 0.65 to 3.8 [18] has become realistic.

For $\gamma \ll 1$, it is commonly referred to as TI, in which the electron can escape from the static barrier formed by the combination of Coulomb potential and laser electric field with non-vanishing probability, even if its energy is lower than the barrier top. Tunneling has become the foundation for many areas of pure and applied science, such as tunnel diodes [19], scanning tunneling microscopy [20], and laser driven electron holography [21, 22]. In the opposite limit of $\gamma \gg 1$, the electron is ionized from atoms by absorbing several photons. This process is termed as MPI.

#355337 https://doi.org/10.1364/OE.27.006471
Journal © 2019 Received 17 Dec 2018; revised 6 Feb 2019; accepted 6 Feb 2019; published 20 Feb 2019

Optics EXPRESS

The intermediate regime ($\gamma \sim 1$) is intuitively considered as the borderline between the TI and MPI. In this regime, the dominant ionization mechanism changes from TI to MPI with the increasing of γ. However, this rough estimation might hamper and even perplex the interpretation of many experimental results, because one cannot explicitly determine which ionization mechanism plays the dominant role at a specific γ. Considering that most of the experiments are performed on atoms with laser intensities and wavelengths far away from two limiting cases ($\gamma \ll 1$ and $\gamma \gg 1$) [18, 23], the identification of TI and MPI in the intermediate ($\gamma \sim 1$) regime becomes necessary. Only a few works have addressed this issue in systematic and quantitative way. Ref. [24, 25] reported the feature of the final momentum distribution of ionized electrons in a numerical way for different γ values, and the dominant ionization mechanism was assigned to different structures qualitatively. Besides, Yudin et al. [26] established a valid closed-form analytical expression for calculating ionization rate at $\gamma \sim 1$ regime. Using this formula the possible "excited" or "virtually excited" path [27, 28] can barely be treated. Moreover, defining a borderline between TI and MPI, the $\gamma \sim 1$ regime raises the heated topic of the existence of nonadiabaticity in the strong-field ionization process. Some recent experiments have shown that TI starts to deviate from the adiabaticity to nonadiabaticity in this intermediate regime, which is also manifested itself on the tunneling ionization time [29], tunneling exit [30, 31], and tunneling initial momentum [32–34]. Therefore, to determine the tunneling initial conditions unambiguously and exclude the contribution from possible multiphoton process, obviously one must maintain experimental conditions in which TI is the dominant process. This requires the quantification of the weight of TI and MPI at a practical laser parameter.

In this paper, we explore the ionization delay time to show the change of dominant ionization mechanisms over a broad range of γ. For different laser intensities, we show that the delay time picture is a good approach to distinguish TI and MPI. In order to confirm the competition of TI and MPI process in intermediate γ regime, we use two Gaussian functions, which have forms following the tunneling and multiphoton ionization rate theory, to iteratively fit the probability current calculated by time dependent Schrödinger equation (TDSE) numerically. The fitting results are clearly evident that the plateau-like structure in ionization delay time picture is actually the weighted average delay time of TI and MPI electrons. We also put forward a quantum-classical approach to quantify the fraction of TI and MPI in the intermediate γ regime, and a good agreement is achieved with the results evaluated by NICFA. Furthermore, the well separated electrons by HQCA allow us to trace the TI and MPI electron dynamics in classical way, which makes dynamical processes of interest visualization. As an example, the separated TI and MPI electrons are classically propagated to reach their asymptotic states, then the reconstructed final momentum reproduces the main features of the TDSE for TI and MPI dominant cases, respectively.

2. Theoretical method

2.1. Solving the time dependent Schrödinger equation for probability current

The wave function is obtained by numerically solving the one or two-dimension TDSE with single-active electron (SAE) approximation (atomic unit is employed throughout),

$$i\partial\psi(\mathbf{r},t)/\partial t = [-\nabla^2/2 + V_C(\mathbf{r}) + V_E(\mathbf{r},t)]\psi(\mathbf{r},t), \tag{1}$$

where $V_E(\mathbf{r},t) = -\mathbf{E}\cdot\mathbf{r}$ is the laser-electron interaction potential under dipole approximation in length gauge. $\mathbf{E}(t)$ is the linearly polarized laser field along the x-axis,

$$\mathbf{E}(t) = E_0 f(t)\cos(\omega t)\hat{\mathbf{x}}. \tag{2}$$

Here, E_0 is the amplitude, and ω is the angular frequency. $f(t) = \sin^2(\pi t/\tau)$ is the pulse envelope and the pulse duration is $\tau = 2T_0$ (the optical cycle $T_0 = 2\pi/\omega$). The atom is exposed

Optics EXPRESS

in this linearly polarized laser field and the magnetic field component is neglected. Those render the motion of the electron quasi-one-dimensional, allowing us to investigate general features of the electron motion in a one or two-dimensional scenario. The soft-core potential $V_C(\mathbf{r}) = -1/(\mathbf{r}^2 + \alpha)^{1/2}$ [35–38] is used to model the essential features of an electron in Coulomb potential. With $\alpha = 2$ for one-dimensional grid and $\alpha = 0.639$ for two-dimensional grid, the ground state has the energy of 0.5 a.u., which is close to the ionization potential of hydrogen atom. We utilize the split-step Fourier method to numerically solve Eq. (1) [39]. To solve one-dimension TDSE, the dimension size is 800 a.u., with a grid step of 0.1 a.u. and a time step of 0.02 a.u.. To solve two-dimension TDSE, the dimension size is 500 a.u., with a grid step of 0.2 a.u. and a time step of 0.02 a.u.. All of the parameters can guarantee that the grid is fine enough to include the detailed evolution of the electron wave packet. The ground state wave function is obtained via imaginary time propagation method [40]. The random initial state is evolved in imaginary time (time step $i\delta t$, $\delta t = 0.02$ a.u.) on the space grid mentioned above. Starting from the ground state, the ionized wave function $\psi(\mathbf{r}_d, t)$ is saved at the fixed radius $\mathbf{r}_d$, where the VDs (virtual detectors) [41, 42] are located. The virtual detector is realized by calculating the probability current at some fixed position in space. After the electron is propagated beyond the VDs, we use an absorbing function $f_{abs}(\mathbf{r}) = 1 - 1/(1 + \exp(-(|\mathbf{r}| - L_c)/r_a))$ to prevent reflection on the boundary of grid. The choice of the parameters (L_a, r_a) satisfies the dominant physical conditions in [43]. The evolutive probability current at $\mathbf{r}_d$ was obtained by

$$\mathbf{j}(\mathbf{r}_d, t) = i[\psi(\mathbf{r}_d, t)\nabla\psi(\mathbf{r}_d, t)^* - c.c]/2, \tag{3}$$

which represents the time dependent net number of the electrons passing the VDs.

2.2. Non-linear iterative curve fitting algorithm

In the past decades, the adiabatic Ammosov-Delone-Krainov (ADK) theory [44] is widely used to calculate the ionization rate of TI, with a simple form of $W(t) \propto \exp(-2(2I_p)^{3/2}/(3E(t)))$. In the case of a linearly polarized field, the ionization rate follows the formula of $W(t) = 4\sqrt{3/(\pi E(t))}\exp(-2/(3E(t)))$ for hydrogen atom [45]. For MPI, the theoretical ionization rate depends on the field strength in form of $W(t) \propto E(t)^{2N}$, and N ($N = I_p/\omega$) is the number of absorbing photons. We find that those theoretical ionization rates of TI and MPI calculated by our short oscillation field are in Gaussian shape, therefore, it is reasonable to utilize two Gaussian functions to simulate the ionization rate (probability current) of TI and MPI. The form of those functions is as follows:

$$fun_{1,2} = a_{1,2} \cdot \exp(-(t - b_{1,2})^2/c_{1,2}^2), \tag{4}$$

where subscript 1 and 2 represent TI and MPI, respectively.

We then carry out the iterative methods in a kind of "trial and error" procedure: (1) Make first guess of all the non-linear parameters; (2) Compute $G = fun_1 + fun_2$ and compare it to the data set so as to calculate a fitting error; (3) If the fitting error is greater than the required fitting accuracy, the program automatically changes the parameters and loops back around to the previous step and repeats until the required fitting error of less than 5% is achieved. The model applied here has four nonlinear variables (the position of maximum value $b_{1,2}$ and width of two Gaussian functions $c_{1,2}$, which are determined by iteration) and two linear variables (the heights of the Gaussian functions $a_{1,2}$, which are determined directly by regression for each trial iteration).

2.3. Hybrid quantum and classical approach

In this work, we introduce a model, which combines the advantages of both TDSE and classical methods. The initial stage of this method obeys quantum principles and the subsequent fast-compute classical stage provides a clear physical picture. The starting point of this hybrid

Optics EXPRESS

approach is to convert the quantum outgoing electron wave packet calculated by numerical integration of the TDSE into classical local momentum $\mathbf{p}(\mathbf{r}_d, t)$ [41, 42, 46] through

$$\mathbf{p}(\mathbf{r}_d, t) = \mathbf{j}(\mathbf{r}_d, t)/|\psi(\mathbf{r}_d, t)|^2. \tag{5}$$

Here, the probability current density $\mathbf{j}(\mathbf{r}_d, t)$ of outgoing electrons is calculated by Eq. (3). Since Eq. (5) is only valid in the case of well-defined momentum of the ionized electron, the VDs are placed far away from the electron oscillation amplitude $R = E_0/\omega^2$ ($\mathbf{r}_d \gg R$). With the known classical position and momentum used as initial conditions, the ionized electrons can be then propagated classically forward to laser end or backward to laser start, using the same Hamiltonian of the TDSE, automatically taking the Coulomb correction into account. The evolution of the electron with the above initial conditions is governed by Newton's equation of motion:

$$d^2\mathbf{r}/dt^2 = \mathbf{E}(t) - \nabla V_C(\mathbf{r}). \tag{6}$$

It is noted that the full quantum treatment before the transformation by VDs enables us to take the electron transition from not only ground state but also excited states into count, without any specific approximations. For the back propagation, the classical electrons could be bounced by the potential barrier, which is a forbidden regime for tunneling electrons, and their trajectories are terminated with the criterion that the electron has tunneled if the electron's displacement in the instantaneous field direction is a minimum, when the particles are back propagated from the position of the VDs toward the nuclei [34].

3. Result and discussion

Figure 1 shows the calculated one-dimension probability current $j(r_d, t)$, when γ is varied in a range covering from 0.6 to 1.8. The laser intensity is fixed at 5.9×10^{13} W/cm^2. We place the VD at r_d by meeting $V(\mathbf{r}, t_0) = -I_p$ [47], where the laser field has maximum value at time t_0 ($t_0 = T_0$), I_p is the ionization potential and $V(\mathbf{r}, t_0)$ is the combined potential of laser field and Coulomb force. One can see that all of the curves dominantly exhibit positive peaks, indicating that the reflection of outgoing electron raised by under-the-barrier dynamics can be neglected. This result also proves that the choice of r_d is reasonable that only truly ionized electrons are detected in this oscillating field. At small γ of 0.6, the probability current just has one peak. However, with the increasing of γ another peak gradually appears, and a dominant double-peak structure is formed. Although there are some minor peaks originated from the laser oscillation, they have small contribution to the total probability current and could be ignored. When γ is further increased to 1.8, the probability current curve changes back to one dominant peak. As we all know, the dominant ionization mechanism at small $\gamma \ll 1$ (large $\gamma \gg 1$) is TI (MPI), therefore the probability current of the ionized wave packet at γ of 0.6 and 1.8 can be unambiguously assigned to TI and MPI, respectively. Intuitively, we can suppose the double-peak structure is caused by the co-existence of TI and MPI in the intermediate γ regime. After a close inspection of the double-peaked structure, we found the relative height of the pre-peak (purple arrows) gradually grows until it becomes completely dominant with the increasing of γ, in contrast to the post-peak (red arrows). This observation is qualitatively consisted with the widely accepted fact that the proportion of MPI is growing when γ is increased, vice versa. In the other words, the relative ratio between MPI and TI increases, because the ionization probability of each channel cannot abruptly change. Although this is just a qualitative separation of TI and MPI peaks, it is enough for us to arrange the Gaussian-form functions fun_1 and fun_2 to the TI and MPI peaks, respectively, getting ready for the next step of nonlinear fitting the whole probability current curve (more discussed in following section). Furthermore, it is also noticed that the peaks of the time-dependent probability current are delayed as γ is increased. We record the electron's weighted average of time t_D of arrival at r_d. While r_d is recognized as the tunneling exit, t_D

Optics EXPRESS

becomes tunneling delay time according in [47]. Here, we emphasize that the location of r_d only serves for recording the numerical observable t_D in our work. Since the actual tunneling delay times are sensitively dependent on how the tunnel exit is chosen [31], we do not assign t_D conforming to any existing concept of tunneling ionization time, such as Mandelstam-Tamm time [48], Keldysh time [14], Wigner time [49]. Instead, the delay time τ_A is obtained through $t_D - t_0$.

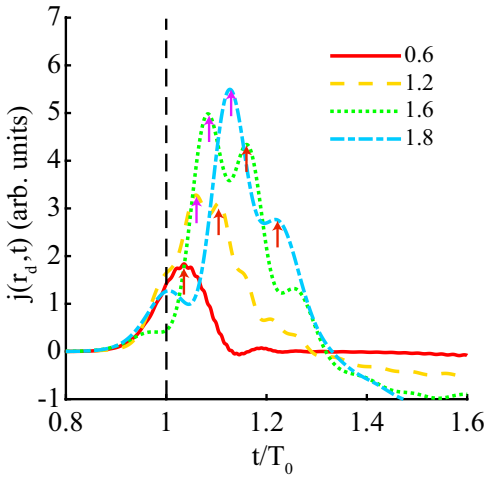

Fig. 1. The probability current $j(r_d, t)$ as a function of time at the detector r_d, at Keldysh parameters of 0.6, 1.2, 1.6, 1.8. The laser intensity is fixed at 5.9×10^{13} W/cm^2. The vertical dashed black line is used to guide the moment when the laser field reaches maximum. The purple arrows and the red arrows represent the pre-peak and post-peak, respectively.

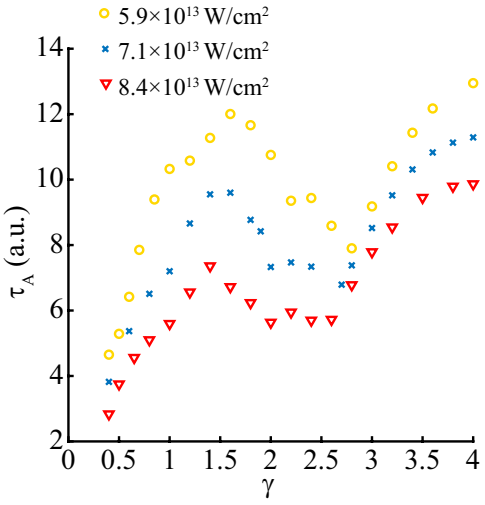

Fig. 2. The delay time τ_A plotted as a function of γ in various intensities: $I = 5.9 \times 10^{13}$ W/cm^2, $I = 7.1 \times 10^{13}$ W/cm^2, and $I = 8.4 \times 10^{13}$ W/cm^2.

For quickly checking the trend of the delay time, we plot the delay time τ_A in one-dimensional grid as a function of γ in three different intensities in Fig. 2. The intensities were chosen not to exceed 10^{14} W/cm^2 in order to avoid barrier suppression ionization. A positive delay time is

Optics EXPRESS

observed for the three intensities, and it generally increases with the growth of γ. After closer inspection, for each constant laser intensity the curve can be divided into three stages: two ascent stages in different growth trend and one pronounced plateau-like stage between them. The detailed understanding of this interesting plateau-like structure in the intermediate γ regime will be discussed later. Conventionally, γ is used to distinguish the ionization regime with small $\gamma \ll 1$ for TI and large $\gamma \gg 1$ for MPI [14]. Therefore, we can assign the regime before and after the plateau-like structure as TI regime and MPI regime undoubtedly. For the first ascent stage in TI regime ($\gamma \ll 1$), the electron tunnels crossing the barrier in phase space without gaining additional energy in the electric field. The observed increase of delay time τ_A with growing γ at constant laser intensity in Fig. 2 is consistent with the fact that the laser pulse duration is decreased correspondingly. The shorter laser pulse duration grants the wave function less time to evolve and to adopt to the time-varying Hamiltonian during the rise of the electric field, therefore, the wave function has shorter time to develop the necessary portion for tunneling, and needs more time to reach the maximum ionization rate. We also find, the delay time tends to zero (not shown) as γ approaches zero. This is in accordance with that the electron is ionized at the laser peak in the frame of adiabatic tunneling picture that electron tunneling doesn't need time. Furthermore, it is also shown that, a lower (higher) electric field strength results in a longer (shorter) delay time at a constant γ. This result agrees well with the Keldysh tunneling time $\tau_k = \sqrt{2I_p}/E_0$ [50], which is the time scale that the bound state under the barrier develops the wave function component necessary for TI. For the second ascent stage in MPI regime ($\gamma \gg 1$), the electron is elevated into an unbound state by absorbing multiple photons. Then it is accelerated by the laser field far away from the parent atom to detector. The electron has the cycle-average kinetic energy $U_p = E_0^2/4\omega^2$ (ponderomotive energy) in the oscillating field. As γ is increased at the constant electric field strength, we find that the delay time τ_A increases. The growing of γ (at constant E_0) corresponds to the increasing of ω and the decreasing of U_p, which makes the ionized electrons slow and need more time to reach the VD. On the other hand, if γ is kept constant, the increasing of E_0 leads to the growing of U_p, and the electron spends less time to the VD.

We now go back to discuss the plateau-like structure in the ionization delay time picture. As shown in Fig. 2, the range of the plateau-like structure reduces and shifts towards smaller γ with the increasing of laser intensity. Since the plateau-like structure is located between the two limiting cases of TI and MPI, one can logically speculate that the formation and change of this plateau are a consequence of a competitive process of TI and MPI.

To demonstrate the prediction, we use NICFA through $G = fun_1 + fun_2$ to fit the probability current calculated by one-dimension TDSE in the intermediate regime, for example, $\gamma = 1.6$ and the laser intensity is 5.9×10^{13} W/cm^2 as shown in Fig. 3(a). By employing the fitting method described in method section, the variables are obtained: $a_1 = 4.27 \times 10^{-4}$, $a_2 = 4.9 \times 10^{-4}$, $b_1 = 111.5$, $b_2 = 103.6$, $c_1 = 3.93$, $c_2 = 4.3$. We justify the validity of this fitting method by comparing the full width of half maximum (FWHM) of $fun_{1,2}$ with those calculated through theoretical TI and MPI rate. For $\gamma = 0.6$ at the laser intensity of 5.9×10^{13} W/cm^2, where TI is dominant, the FWHM of 22.48 a.u. calculated by ADK theory is in reasonable agreement with FWHM of 25.01 a.u. for fun_1. The deviation may originate from residual nonadiabaticity which makes the true wavepacket wider than that predicted by static ADK [32]. For $\gamma = 2.8$ at the laser intensity of 5.9×10^{13} W/cm^2, the lowest order of ionization is a 5-photon process. The FWHM of fun_2 is 7.76 a.u. larger than 5.99 a.u. calculated by the MPI rate. This difference may originate from the diffusion of wavepacket in the oscillating field when the electron wavepacket is propagated from the ion core to the VD. Then we calculate the fitting delay time $b_{1,2} - t_0$ of TI and MPI in the interested intermediate regime by changing γ from 1 to 2.6 at 5.9×10^{13} W/cm^2 as shown in Fig. 3(b). We can see that the fitting delay time of TI (MPI) in intermediate regime agrees well with the growth trend of delay time of TI (MPI) regime. Moreover, we verify that the delay time in the intermediate regime (plateau-like structure) is a weighted average of the

Optics EXPRESS

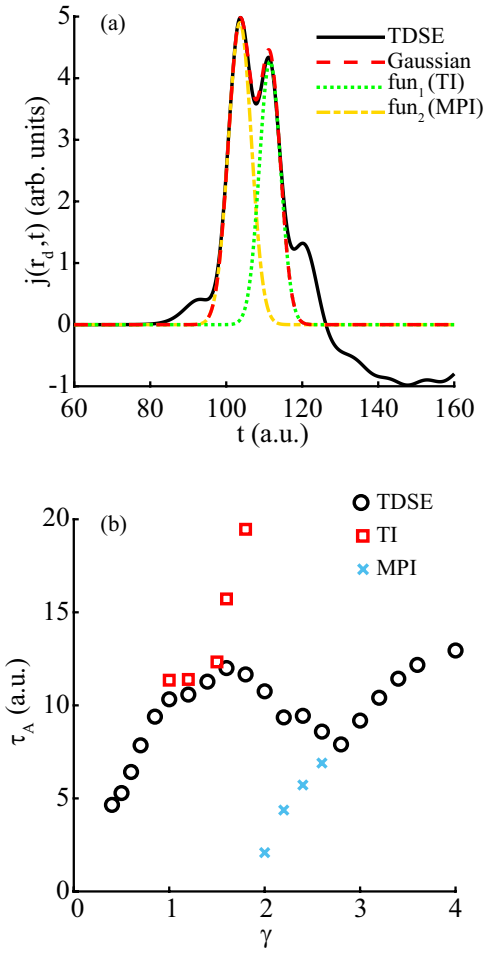

Fig. 3. (a) The probability current $j(r_d, t)$ as a function of time at the detector r_d, where $\gamma = 1.6$ and the laser intensity is 5.9×10^{13} W/cm^2 (black curve). The red dashed curve is a Gaussian fit to the probability current. The green dotted curve and yellow dash-dotted curve are Gaussian fitting of TI and MPI, respectively. (b) The delay time covering a range of Keldysh parameters from 0.4 to 4 at laser intensity of 5.9×10^{13} W/cm^2 (black circles). The red squares and the blue crosses represent the delay time abstracted from the Gaussian fit of probability current of TI and MPI, respectively.

fitting delay time of TI and MPI. In addition, to show our method is generalized, we also try to decouple the TI and MPI electrons launched by a twelve-cycle laser pulses. We again first check the validity of Gaussian type functions for representing the TI and MPI wave packets in the case of using longer laser pulse. For instance, for the limiting case of $\gamma = 0.3$ and $\gamma = 3$ at laser intensity of 5.9×10^{13} W/cm^2, the FWHM calculated by ADK theory (MPI rate) is 49.45 (5.99) a.u., in reasonable agreement with FWHM of 49.95 (8.13) a.u. for the fitted Gaussian function by employing a twelve-cycle laser field. Then the total probability is decoupled into TI and MPI fractions by performing NICFA, and we also extract the delay time from the Gaussian fit of the probability current in the intermediate regime and find no substantial difference compared to the case of two-cycle laser pulse. With the agreement, we can conclude that the plateau-like structure is a consequence of a competitive process of TI and MPI in the intermediate regime for both cases of short and long laser pulses.

Optics EXPRESS

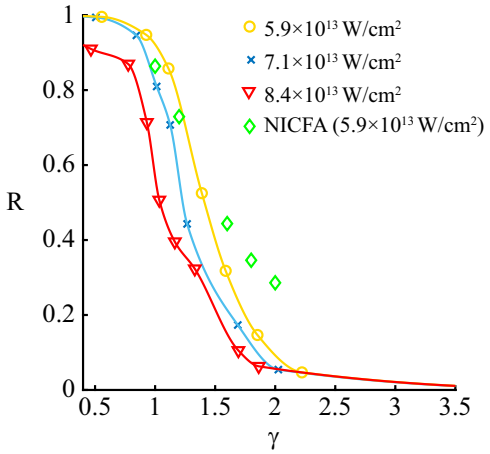

Fig. 4. The fraction of TI electrons in the total ionization electrons (R) as a function of γ at laser intensities: 8.4×10^{13} W/cm^2 (red triangles and curve), 7.1×10^{13} W/cm^2 (blue crosses and curve) and 5.9×10^{13} W/cm^2 (yellow circles and curve). The green rhombuses represent the R calculated by NICFA at laser intensity of 5.9×10^{13} W/cm^2.

To further check the competition between TI and MPI in the intermediate regime, we calculate the fraction of TI in total ionization. We use one-dimension HQCA to obtain the weight of TI electrons P_{tun}. For MPI, the ionized electrons, which are ionized at the ion core via absorbing a certain number of photons, have total energy more than the potential barrier. Therefore, there is no forbidden area for MPI electrons during classical back-propagation. In this case, the back-propagation electrons that fail to be bounced by the combined field are identified as MPI electrons with weights P_{multi}. Here the VD method makes the calculation of ionization dynamics driven by very long wavelength laser feasible at the cost of sacrificing time to replace the finite space, compared with Ref. [51]. More details are described in [34].

We define the fraction of TI electrons as $R = P_{tun}/P_{ion}$, where the total ionization weight $P_{ion} = P_{tun} + P_{multi}$. Subsequently, we plot R as a function of γ in three different intensities. As shown in Fig. 4, R has the same trend for three different intensities. At limiting case of $\gamma \ll 1$, R is almost close to unity and the pure tunneling scenario applies. As γ is increased, the MPI is beginning to take effect, therefore R monotonously decreases in the intermediate regime. This regime can be recognized as the transition from TI to MPI. When R decreases close to zero, the MPI regime is completely dominant at rather large γ. If we define a criterion that $R > 90\%$ and $R < 10\%$ are demarcated as ranges of pure TI and MPI, respectively, the corresponding γ values can be read out from Fig. 4 and the turning points are signed by γ_1, γ_2. For $I = 8.4 \times 10^{13}$ W/cm^2, We extract 0.55 (γ_1) and 1.7 (γ_2) from the red curve in Fig. 4. Similarly, the intermediate regime corresponding $10\% < R < 90\%$ is 0.91 to 1.85 at $I = 7.1 \times 10^{13}$ W/cm^2 and 1.04 to 1.98 at $I = 5.9 \times 10^{13}$ W/cm^2. We can find that the lower turning point γ_1 shifts up by 0.49 while the higher turning point γ_2 changes by 0.28, when the applied laser intensities are decreased from $I = 8.4 \times 10^{13}$ W/cm^2 to $I = 5.9 \times 10^{13}$ W/cm^2. The other remarkable feature we read out from Fig. 4 is that the tunneling fraction shows substantial discrepancy at the same γ but different laser intensity in intermediate regime. For example, the tunneling fractions is 35% and 18%, when γ is 1.55 for two different intensities of 5.9×10^{13} W/cm^2 and 8.4×10^{13} W/cm^2. Those suggest that characterizing the dominant ionization mechanism according to the value of γ is fundamentally unreliable unless at one of the extreme cases. Though the intermediate regime between γ_1 and γ_2 changes with different laser intensities, γ_1 and γ_2 values reasonably agree with γ values referred by both ends of the plateau-like structure shown in Fig. 2. In other word,

Optics EXPRESS

the regime which is responsible for the transition from TI to MPI mechanism is well defined by the plateau-like structure in the ionization delay time trend. To check the self-consistency, we further compare the tunneling fraction R calculated by HICFA (green rhombuses, the total ionization rate of TI (MPI) electrons is calculated through the time integration of $fun_{1,2}$) with HQCA (yellow circles and curve) as illustrated in Fig. 4, and they match each other well.

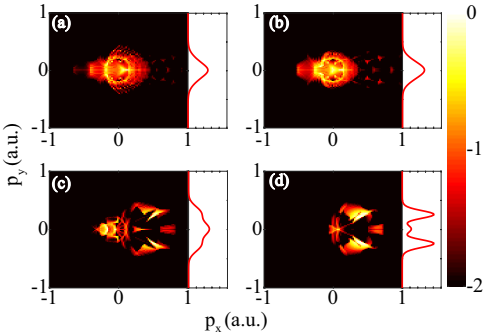

Fig. 5. The two-dimension reconstructed final momentum distribution of tunneling electrons at various Keldysh parameters: (a) $\gamma = 0.84$; (b) $\gamma = 0.92$; (c) $\gamma = 1.45$ and (d) $\gamma = 1.69$. The laser intendity is fixed at 7.1×10^{13} W/cm^2. The weights of the electrons are counted in a logarithmic scale. Furthermore, the side profile is the integrated signal along the polarization axis which is used to show the feature of p_y, and the weight is determined by normalization of the integral value.

From a practical point of view, one could also be interested in the behavior of the well defined TI and MPI electrons in electric field as well as their final momentum distribution. To show the typical features of TI and MPI, we calculate the electron momentum, using the same method mentioned above in two-dimension space. The electrons of TI and MPI are first separated via HQCA, and then the two kinds of electrons are propagated forward to the end of laser in classical way. Figure 5 shows the reconstructed final momentum distribution of TI. Since we apply a linearly polarized laser field, the final lateral momentum p_y (side profile) remains unchanged with respect to its ionization initial momentum p_y^0, if Coulomb interaction can be neglected. For relatively smaller γ of 0.84 and 0.92, respectively, as illustrated in Figs. 5(a) and 5(b), the observed p_y has a Gaussian-like distribution centered at zero. This result is self-consistent with the popular prediction made by many classical trajectory Monte Carlo (CTMC) simulations [52, 53] that the initial tunneling velocity perpendicular to instantaneous field has a zero centered Gaussian-like distribution in adiabatic TI case. Conversely, at relatively larger γ of 1.45 and 1.69 in Figs. 5(c) and 5(d), p_y is peaked around a nonzero value as a consequence of nonadiabatic effect of the TI dynamics, which is rooted in the absorption of energy from the time-varying barrier [54, 55]. As γ is increased, p_y has a more obvious deviation from zero due to more pronounced nonadiabtic effect. For instance, we can read out that $p_y = 0.21$ a.u. at $\gamma = 1.45$, smaller than 0.25 a.u. at $\gamma = 1.69$.

Bear in mind that the electric field here is an oscillating field with zero vector potential at the end of the laser $A(\infty) = 0$. So the final longitudinal momentum along laser polarized x-axis direction complying with the canonical momentum conservation law is given by $p_x(\infty) = p_x(t_i) + A(t_i)$. $p_x(t_i)$ and $A(t_i)$ are the momentum and the vector potential of laser at the instant of electron's ionization. For adiabatic tunneling ionization at γ of 0.84 and 0.92 as illustrated in Figs. 5(a) and 5(b), p_x almost has a distribution centered at the zero value, which is in fact very close to the vector potential at t_0, $A(t_0) = 0$. This means that the electron tunnels out with near zero initial longitudinal momentum at the instant of laser peak, which is in accord with the adiabatic ADK theory [44]. Moreover, the tiny deviation of the center of p_x from $A(t_0)$ is present as well,

Optics EXPRESS

which is due to the freed electron pulled by its parent ion through Coulomb interaction. As displayed in Figs. 5(c)–(d), when γ is increased from 1.45 to 1.69, the center of p_x shifts towards nonzero value and gradually departs even further from $A(t_0)$. One can also attribute this result to a stronger Coulomb interaction, but the mechanism behind is two-fold. First, the ionized electron is slower in a laser field with smaller U_p, and therefore the Coulomb force acts on electron for longer time. Second, due to the nonadiabatical TI, the tunneling exit shifts closer to the ion core [31], hence, Coulomb attraction becomes stronger.

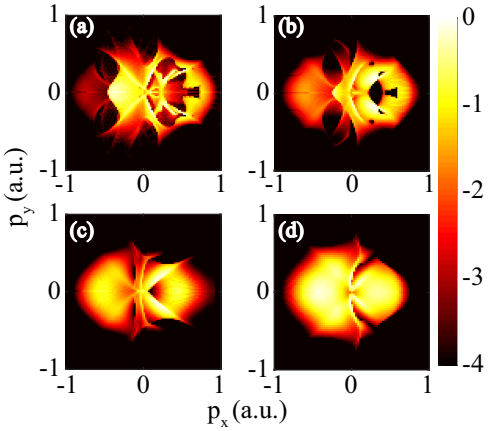

Fig. 6. The two-dimension reconstructed final momentum distribution of MPI at various Keldysh parameters: (a) $\gamma = 1.69$; (b) $\gamma = 2.03$; (c) $\gamma = 2.53$; (d) $\gamma = 3.38$. The laser intensity is fixed at 7.1×10^{13} W/cm^2. The weights of the electrons are in logarithmic scale.

Now we turn to the reconstructed final momentum of MPI electrons, as shown in Fig. 6. The electrons ionized from MPI-process are governed by the energy conservation law $p_0^2/2 = (n_0 + s)\omega - I_p - U_p$, where n_0 is the minimum number of absorbing photons, s is the additional number of photons. At first glance of Fig. 6, the general ATI peaks are absent because there is no interference of electrons born within the different cycles of the laser pulse. For all γ, p_y has a distribution centered at zero, suggesting that the ionization is directly from the initial state with $s = 0$. One can also see from Fig. 6 that the spread of p_y becomes broader with the increasing of γ, which means that the maximum of p_y^0 increases. At the constant laser intensity, an increase in γ corresponds to an increase in photon energy and decrease of U_p, causing a larger maximum value of p_y^0.

Regarding to the distribution of final longitudinal momentum p_x, one may notice that in Fig. 6(a), there seems to be missing parts. Those missing parts are nothing else but the tunneling ionized electrons that have been identified in Fig. 5(d). If γ is further increased, the missing parts gradually appear in Figs. 6(c) and 6(d). Because at large enough γ, the tunneling fraction is so small that the almost pure MPI is achieved. In this case, the MPI electron's momentum distributes along not only x-axis but also y-axis, which indicates that the photoelectron distribution of MPI is independent on the polarized direction of laser field. It is different from the tunneling electron's momentum, which spreads along the polarized direction of laser field as shown in Fig. 5. This shows good agreement with the ionization spectra in [56].

4. Conclusion

We have shown a pronounced plateau-like structure in the delay time picture, which can be defined as the borderline of the intermediate regime between TI and MPI. The plateau-like structure is caused by a competition between TI and MPI, which is verified with both of HICFA and HQCA.

Optics EXPRESS

The quantitative definition of the intermediate regime is helpful to disentangle the dominant contribution from TI and MPI in practical experiment condition. Furthermore, the well separated TI (MPI) electrons are propagated forwards for reconstructing their final momentum, which will be beneficial to analysis detailed evolution dynamics of electrons in different ionization channels.

Funding

National Natural Science Foundation of China (NSFC) (11574101, 11627809, 11774111).

References

1. K. Ishikawa, "Photoemission and ionization of He^+ under simultaneous irradiation of fundamental laser and high-order harmonic pulses," Phys. Rev. Lett. **91**, 043002 (2003).
2. L. He, P. Lan, A. T. Le, B. Wang, B. Wang, X. Zhu, P. Lu, and C. D. Lin, "Real-Time Observation of Molecular Spinning with Angular High-Harmonic Spectroscopy," Phys. Rev. Lett. **121**, 163201 (2018).
3. F. Krausz and M. Ivanov, "Attosecond physics," Rev. Mod. Phys. **81**, 163–234 (2009).
4. M. Wickenhauser, X. M. Tong, D. G. Arbó, J. Burgdörfer, and C. D. Lin, "Signatures of tunneling and multiphoton ionization in the electron-momentum distributions of atoms by intense few-cycle laser pulses," Phys. Rev. A **74**, 041402 (2006).
5. C. I. Blaga, F. Catoire, P. Colosimo, G. G. Paulus, H. G. Muller, P. Agostini, and L. F. DiMauro, "Strong-field photoionization revisited," Nat. Phys. **5**, 335–338 (2009).
6. F. Lindner, M. G. Schatzel, H. Walther, A. Baltuska, E. Goulielmakis, F. Krausz, D. B. Milosevic, D. Bauer, W. Becker, and G. G. Paulus, "Attosecond double-slit experiment," Phys. Rev. Lett. **95**, 040401 (2005).
7. F. Grasbon, G. G. Paulus, H. Walther, P. Villoresi, G. Sansone, S. Stagira, M. Nisoli, and S. De Silvestri, "Above-threshold ionization at the few-cycle limit," Phys. Rev. Lett. **91**, 173003 (2003).
8. J. Shah, *Ultrafast spectroscopy of semiconductors and semiconductor nanostructures* (Springer Science and Business Media, 2013).
9. D. S. Chemla, "Nonlinear optics in quantum-confined structures," Phys. Today **46**, 46–52 (1993).
10. S. C. Jones, P. Braunlich, R. T. Casper, X. Shen, and P. Kelly, "Recent progress on laser-induced modifications and intrinsic bulk damage of wide-gap optical materials," Opt. Engineering **28**, 281039 (1989).
11. L. Li, P. Lan, X. Liu, L. He, X. Zhu, O. D. Mücke, and P. Lu, "Method for direct observation of Bloch oscillations in semiconductors," Opt. Express **26**, 23844–23853 (2018).
12. X. Zhang, X. Zhu, D. Wang, L. Li, X. Liu, Q. Liao, P. Lan, and P. Lu, "Ultrafast oscillating-magnetic-field generation based on electronic-current dynamics," Phys. Rev. A **99**, 013414 (2019).
13. C. Qin, L. Yuan, B. Wang, S. Fan, and P. Lu, "Effective electric-field force for a photon in a synthetic frequency lattice created in a waveguide modulator," Phys. Rev. A **97**, 063838 (2018).
14. L. Keldysh, "Ionization in the field of a strong electromagnetic wave," Sov. Phys. JETP **20**, 1307–1314 (1965).
15. N. Ishii, K. Kaneshima, K. Kitano, T. Kanai, S. Watanabe, and J. Itatani, "Carrier-envelope phase-dependent high harmonic generation in the water window using few-cycle infrared pulses," Nat. Commun. **5**, 3331 (2014).
16. Z. Hong, Q. Zhang, and P. Lu, "Compact dual-crystal optical parametric amplification for broadband IR pulse generation using a collinear geometry," Opt. Express **21**, 9491–9504 (2013).
17. Z. Hong, Q. Zhang, P. Lan, and P. Lu, "Generation of few-cycle infrared pulses from a degenerate dual-pump OPCPA," Opt. Express **22**, 5544–5557 (2014).
18. R. Boge, C. Cirelli, A. S. Landsman, S. Heuser, A. Ludwig, J. Maurer, M. Weger, L. Gallmann, and U. Keller, "Probing nonadiabatic effects in strong-field tunnel ionization," Phys. Rev. Lett. **111**, 103003 (2013).
19. L. Esaki and R. Tsu, "Superlattice and negative differential conductivity in semiconductors," IBM J. Res. Dev. **14**, 61–65 (1970).
20. G. Binnig, H. Rohrer, C. Gerber, and E. Weibel, "7 × 7 Reconstruction on Si(111) Resolved in Real Space," Phys. Rev. Lett. **50**, 120–123 (1983).
21. O. I. Tolstikhin, T. Morishita, and L. B. Madsen, "Theory of tunneling ionization of molecules: Weak-field asymptotics including dipole effects," Phys. Rev. A **84**, 053423 (2011).
22. J. Tan, Y. Zhou, M. He, Y. Chen, Q. Ke, J. Liang, X. Zhu, M. Li, and P. Lu, "Determination of the Ionization Time Using Attosecond Photoelectron Interferometry," Phys. Rev. Lett. **121**, 253203 (2018).
23. M. Uiberacker, T. Uphues, M. Schultze, A. J. Verhoef, V. Yakovlev, M. F. Kling, J. Rauschenberger, N. M. Kabachnik, H. Schroder, M. Lezius, K. L. Kompa, H. G. Muller, M. J. Vrakking, S. Hendel, U. Kleineberg, U. Heinzmann, M. Drescher, and F. Krausz, "Attosecond real-time observation of electron tunnelling in atoms," Nature **446**, 627–632 (2007).
24. T. Marchenko, Y. Huismans, K. J. Schafer, and M. J. J. Vrakking, "Criteria for the observation of strong-field photoelectron holography," Phys. Rev. A **84**, 053427 (2011).
25. T. Topcu and F. Robicheaux, "Dichotomy between tunneling and multiphoton ionization in atomic photoionization: Keldysh parameter γ versus scaled frequency Ω," Phys. Rev. A **86**, 053407 (2012).
26. G. L. Yudin and M. Y. Ivanov, "Nonadiabatic tunnel ionization: Looking inside a laser cycle," Phys. Rev. A **64**, 013409 (2001).

Optics EXPRESS

27. M. Klaiber and J. S. Briggs, "Crossover from tunneling to multiphoton ionization of atoms," Phys. Rev. A **94**, 053405 (2016).
28. E. E. Serebryannikov and A. M. Zheltikov, "Strong-Field Photoionization as Excited-State Tunneling," Phys. Rev. Lett. **116**, 123901 (2016).
29. P. Eckle, A. N. Pfeiffer, C. Cirelli, A. Staudte, R. Dörner, H. G. Muller, M. Buttiker, and U. Keller, "Attosecond ionization and tunneling delay time measurements in helium," Science **322**, 1525–1529 (2008).
30. M. Klaiber, E. Yakaboylu, H. Bauke, K. Z. Hatsagortsyan, and C. H. Keitel, "Under-the-barrier dynamics in laser-induced relativistic tunneling," Phys. Rev. Lett. **110**, 153004 (2013).
31. M. Klaiber, K. Z. Hatsagortsyan, and C. H. Keitel, "Tunneling dynamics in multiphoton ionization and attoclock calibration," Phys. Rev. Lett. **114**, 083001 (2015).
32. L. Arissian, C. Smeenk, F. Turner, C. Trallero, A. V. Sokolov, D. M. Villeneuve, A. Staudte, and P. B. Corkum, "Direct test of laser tunneling with electron momentum imaging," Phys. Rev. Lett. **105**, 133002 (2010).
33. D. Ye, X. Liu, and J. Liu, "Classical trajectory diagnosis of a fingerlike pattern in the correlated electron momentum distribution in strong field double ionization of helium," Phys. Rev. Lett. **101**, 233003 (2008).
34. Q. Zhang, G. Basnayake, A. Winney, Y. Lin, D. Debrah, S. K. Lee, and W. Li, "Orbital-resolved nonadiabatic tunneling ionization," Phys. Rev. A **96**, 023422 (2017).
35. Q. Su and J. H. Eberly, "Model atom for multiphoton physics," Phys. Rev. A **44**, 5997–6008 (1991)
36. R. L. Hall, N. Saad, K. D. Sen, and H. Ciftci, "Energies and wave functions for a soft-core Coulomb potential," Phys. Rev. A **80**, 032507 (2009).
37. C. W. Clark, "Closed-form solutions of the Schrödinger equation for a class of smoothed Coulomb potentials," J. Phys. B: At. Mol. Opt. Phys. **30**, 2517–2527 (1997).
38. W.C. Liu and C.W. Clark, "Closed-form solutions of the Schrödinger equation for a model one-dimensional hydrogen atom," J. Phys. B : At. Mol. Opt. Phys. **25**, L517–L524 (1992).
39. M. D. Feit, J. A. Fleck, and A. Steiger, "Solution of the schrödinger equation by a spectral method," J. Comput. Phys. **47**, 412–433 (1982).
40. M. Protopapas, C. H. Keitel, and P. L. Knight, "Atomic physics with super-high intensity lasers," Rep. Prog. Phys. **60**, 389–486 (1997).
41. X. Wang, J. Tian, and J. H. Eberly, "Extended Virtual Detector Theory for Strong-Field Atomic Ionization," Phys. Rev. Lett. **110**, 243001 (2013).
42. B. Feuerstein and U. Thumm, "On the computation of momentum distributions within wavepacket propagation calculations," J. Phys. B **36**, 707–716 (2003).
43. S. Chelkowski, C. Foisy, and A. D. Bandrauk, "Electron-nuclear dynamics of multiphoton H_2^+ dissociative ionization in intense laser fields," Phys. Rev. A **57**, 1176–1185 (1998).
44. M. V. Ammosov, N. B. Delone, and V. P. Krainov, "Tunnel Ionization Of Complex Atoms And Atomic Ions In Electromagnetic Field," Sov. Phys. JETP **64**, 1191–1194 (1986).
45. N. B. Delone and V. P. Krainov, "Tunneling and barrier-suppression ionization of atoms and ions in a laser radiation field," Phys. Usp. **41**, 469-485 (1998).
46. K. Liu, H. Ni, K. Renziehausen, J. M. Rost, and I. Barth, "Deformation of Atomic $p_\pm$ Orbitals in Strong Elliptically Polarized Laser Fields: Ionization Time Drifts and Spatial Photoelectron Separation," Phys. Rev. Lett. **121**, 203201 (2018).
47. N. Teeny, E. Yakaboylu, H. Bauke, and C. H. Keitel, "Ionization Time and Exit Momentum in Strong-Field Tunnel Ionization," Phys. Rev. Lett. **116**, 063003 (2016).
48. L. Mandelstam and I. Tamm, *The uncertainty relation between energy and time in non-relativistic quantum mechanics* (Springer, 1991).
49. E. Yakaboylu, M. Klaiber, and K. Z. Hatsagortsyan, "Wigner time delay for tunneling ionization via the electron propagator," Phys. Rev. A **90**, 012116 (2014).
50. G. Orlando, C. R. McDonald, N. H. Protik, G. Vampa, and T. Brabec, "Tunnelling time, what does it mean?" J. Phys. B: At. Mol. Opt. Phys. **47**, 204002 (2014).
51. H. Ni, U. Saalmann, and J. M. Rost, "Tunneling Ionization Time Resolved by Backpropagation," Phys. Rev. Lett. **117**, 023002 (2016).
52. B. Hu, J. Liu, and Shi-gang Chen, "Plateau in above-threshold-ionization spectra and chaotic behavior in rescattering processes," Phys. Lett. A **236**, 533–542 (1997).
53. J. S. Cohen, "Reexamination of over-the-barrier and tunneling ionization of the hydrogen atom in an intense field," Phys. Rev. A **64**, 043412 (2001).
54. V. Mur, S. Popruzhenko, and V. Popov, "Energy and momentum spectra of photoelectrons under conditions of ionization by strong laser radiation (the case of elliptic polarization)," J. Exp. Theor. Phys. **92**, 777–788 (2001).
55. A. Perelomov, V. Popov, and M. Terent'ev, "Ionization of atoms in an alternating electric field," Sov. Phys. JETP **23**, 924-934 (1966).
56. D. I. Bondar, "Instantaneous multiphoton ionization rate and initial distribution of electron momentum," Phys. Rev. A **78**, 015405 (2008).